Am J Physiol Heart Circ Physiol
280: H2103–H2115, 2001.

Gap junctions in the rabbit sinoatrial node

SANDER VERHEULE, MARJAN J. A. VAN KEMPEN,
SJOERD POSTMA, MARTIN B. ROOK, AND HABO J. JONGSMA
Department of Medical Physiology and Sports Medicine,
Utrecht University, 3531 HR Utrecht, The Netherlands

Received 12 May 1999; accepted in final form 7 December 2000

Verheule, Sander, Marjan J. A. van Kempen, Sjoerd Postma, Martin B. Rook, and Habo J. Jongsma. Gap junctions in the rabbit sinoatrial node. *Am J Physiol Heart Circ Physiol* 280: H2103–H2115, 2001.—In comparison to the cellular basis of pacemaking, the electrical interactions mediating synchronization and conduction in the sinoatrial node are poorly understood. Therefore, we have taken a combined immunohistochemical and electrophysiological approach to characterize gap junctions in the nodal area. We report that the pacemaker myocytes in the center of the rabbit sinoatrial node express the gap junction proteins connexin (Cx)40 and Cx46. In the periphery of the node, strands of pacemaker myocytes expressing Cx43 intermingle with strands expressing Cx40 and Cx46. Biophysical properties of gap junctions in isolated pairs of pacemaker myocytes were recorded under dual voltage clamp with the use of the perforated-patch method. Macroscopic junctional conductance ranged between 0.6 and 25 nS with a mean value of 7.5 nS. The junctional conductance did not show a pronounced sensitivity to the transjunctional potential difference. Single-channel recordings from pairs of pacemaker myocytes revealed populations of single-channel conductances at 133, 202, and 241 pS. With these single-channel conductances, the observed average macroscopic junctional conductance, 7.5 nS, would require only 30–60 open gap junction channels.

connexin; sinus node; electrophysiology; immunohistochemistry

THE SINOATRIAL (SA) node serves as the normal pacemaker of the mammalian heart. Activation maps obtained using microelectrodes have shown that each beat is initiated in the central, "dominant" region of the node and spreads with increasing velocity toward the right atrium (4). Pacemaker activity results from the combination of ionic channels expressed by nodal myocytes, which have been studied extensively using the voltage-clamp technique (55). However, isolated pacemaker myocytes show a large variation in beating frequency, whereas in the intact node, all pacemaker cells share a common frequency. It is generally believed that synchronization of nodal pacemaker cells is mediated by electrical coupling through gap junction channels (33). The observation that the conduction velocity is an order of magnitude lower in the center of the node than in the atrial and ventricular working myocardium suggests that electrical coupling between pacemaker myocytes is relatively weak (9, 30). This supposed high intercellular resistance is corroborated by ultrastructural studies of the intercellular contacts between pacemaker cells (32), in which gap junctional plaques were reported to be sparse and small compared with those in the working myocardium (for review see Ref. 38).

Gap junction channels are formed by connexin (Cx) subunits. The Cx family is a large multigene family, of which ≥13 members are known in mammals (18). Gap junction channels consisting of a single type of Cx protein (homomeric channels) have been shown to differ in biophysical and regulational properties (see Ref. 7 for overview). In the mammalian heart, mRNA for Cx37, Cx40, Cx43, Cx45, and Cx46 has been detected (23, 27, 40, 41). Within the heart, different cell types express different Cx proteins. In most species investigated, Cx40 and Cx43 are expressed in atrial myocytes. In the ventricular working myocardium, Cx43 is expressed, and the ventricular conduction system also expresses Cx40 (for review see Ref. 20). Expression of Cx45 in atrial and ventricular myocytes has been reported for the rabbit, dog, and human (12, 27, 50). In contrast, Coppen et al. (10) recently presented evidence that Cx45 expression within the ventricles of rat and mouse is confined to the ventricular conduction system. Cx37 and Cx40 are expressed by endothelial and endocardial cells (41, 50). No reports exist on the localization of Cx46 within the heart, but it could not be detected in the human SA node (12).

The Cx types expressed in nodal pacemaker cells remain a subject of some controversy. In the rabbit and hamster SA nodes, Cx43 has been detected (1, 44), but in the rat, cow, and human, it was reported to be absent (28, 37; for overview see Ref. 38). In the dog, Cx40 was detected in the central nodal area (31). In addition, strands of anti-Cx43-positive myocytes that penetrate the nodal area from the atrium were observed in the guinea pig (47). In the dog, similar strands expressed Cx43 and Cx45 (31). These strands might form a specialized conduction pathway to direct the electrical impulse from the central node to the atrium. More recently, Coppen et al. (11) demonstrated

Address for reprint requests and other correspondence: S. Verheule, Krannert Institute of Cardiology, 1111 West 10th St., Indianapolis, IN 46202 (E-mail: sverheul@iupui.edu).

The costs of publication of this article were defrayed in part by the payment of page charges. The article must therefore be hereby marked "*advertisement*" in accordance with 18 U.S.C. Section 1734 solely to indicate this fact.

that Cx40 and Cx45 are expressed in the central region of the rabbit SA node. These authors reported that bundles of Cx43-expressing atrial myocytes penetrate the SA node. Interestingly, Cx43 and Cx45 were coexpressed in a restricted zone at the endocardial side of the nodal-crista terminalis border (11).

A number of reports have described preparations in which the impulse conduction in the SA node could be studied in some detail (5, 9, 25, 30). However, these studies describe measurements on the complete SA node or strips of nodal tissue. Therefore, interpretation of these results is complicated by the heterogeneity of the nodal area, especially with regard to the complex interface between the atrium and the SA node. The properties of gap junctions can be assessed more directly by the double whole cell voltage-clamp technique (36, 51). In recent years, this technique has been used to study gap junction channels in a large variety of cell types (for review see Ref. 7). However, to our knowledge, there has been only one report of its application to cells isolated from the SA node (1). Anumonwo et al. (1) showed that nodal pairs have a relatively high intercellular resistance and that the single-channel conductance and the sensitivity to the transjunctional potential difference (V_j) are in agreement with those of channels formed by Cx43, the presence of which was demonstrated by immunocytochemistry.

Modifications of the double whole cell voltage-clamp technique have been used to investigate the synchronization of pacemaker cells. Two physically unconnected pacemaker myocytes have been coupled via a microcomputer acting as an artificial gap junction (49), or a single myocyte was coupled to a computer simulating another pacemaker cell (56). These studies provide information on the relation between coupling conductance and the synchronization of pacemaker myocytes, but in these simulations, the junctional conductance (G_j) was represented as an ohmic resistor. For a better understanding of pacemaker synchronization, the biophysical properties of nodal gap junctions and their regulation have to be studied in more detail.

We have studied gap junctions in the adult rabbit SA node with immunohistochemical techniques and double whole cell voltage clamp. We present evidence that central pacemaker myocytes in the rabbit SA node express Cx40 and Cx46. This area is connected to the right atrium via strands of cells that resemble pacemaker myocytes in morphology and express Cx43. Expression of Cx45 was not assessed in this study. We demonstrate that pairs of pacemaker myocytes have a low G_j that is relatively insensitive to V_j. In addition, a population of single-channel conductances that we did not observe in rabbit ventricular or atrial myocyte pairs was present in pacemaker myocyte pairs, probably corresponding to channels formed by Cx46.

METHODS

Myocyte isolation. Adult male New Zealand White rabbits (1,800–2,000 g) were anesthetized by injection of 1.5–2.5 ml of pentobarbital sodium (60 mg/ml; Nembutal, Sanofi Sante) in the marginal ear vein together with 0.3 ml of heparin (5,000 IU/ml, Leo). The excised heart was retrogradely perfused with normal modified Tyrode solution for 5 min and with zero-Ca^{2+} modified Tyrode solution for 3 min. Subsequently, the area bordered by the interatrial septum, crista terminalis, and superior and inferior venae cavae was excised and cut in 1-mm-wide strips, perpendicular to the crista terminalis, with care taken to leave ~1 mm of the crista terminalis attached to the strips. These strips were gently triturated in zero-Ca^{2+} modified Tyrode solution containing 1 mg/ml collagenase B (Boehringer), 0.1 mg/ml protease (Sigma Chemical), and 0.03 mg/ml elastase (Sigma Chemical) for 12 min. The solution was then changed to modified Kraftbrühe solution, and tissue fragments were triturated rigorously for 6 min to release isolated cells. These cells were plated at low density on 35-mm tissue culture dishes (Falcon 3801 Primaria, Becton Dickinson) in modified Kraftbrühe solution. Cells were used for electrophysiological recording 1–7 h after isolation, and the modified Kraftbrühe solution was exchanged for normal modified Tyrode solution ≥30 min before an experiment.

Composition of the salines was as follows: Normal modified Tyrode solution consisted of (in mmol/l) 140 NaCl, 5.4 KCl, 1.8 $CaCl_2$, 1 $MgCl_2$, 6 glucose, and 6 HEPES, with pH adjusted to 7.4 with NaOH. Zero-Ca^{2+} modified Tyrode solution contained (in mmol/l) 120 NaCl, 10 KCl, 1.2 KH_2PO_4, 1.2 $MgSO_4$, 20 glucose, 6 HEPES, 10 taurine, and 6 creatine, with pH adjusted to 7.2 with NaOH. Modified Kraftbrühe solution was made up of (in mmol/l) 85 KCl, 30 KH_2PO_4, 5 $MgSO_4$, 5 pyruvate, 5 creatine, 30 taurine, 20 glucose, 5 succinate, 5 sodium hydroxybutyrate, 2 Na_2ATP, and 2 EGTA, with pH adjusted to 7.0 with KOH.

Immunochemistry. For immunohistochemistry, the SA nodal area was excised from the heart, pinned to a silicone rubber pad, and frozen rapidly in liquid nitrogen. After removal of the rubber pad, 10-mm-thick cryosections were cut in the plane perpendicular to the crista terminalis. For immunocytochemistry, isolated cells were plated on glass coverslips. After 1 h, these cells were fixed by a 5-min incubation in 100% methanol at −20°C. SA nodes from three rabbits were used for immunohistochemistry, and isolated nodal cells from five rabbits were used for immunocytochemistry.

To detect Cx37, Cx40, and Cx43, rabbit polyclonal antibodies (kindly provided by Dr. D. Gros, Dept. of Biology, University of Aix-Marseille II, Aix-Marseille, France) were used. Anti-Cx46 antibody was kindly provided by Dr. D. L. Paul (Dept. of Neurobiology, Harvard Medical School, Boston, MA). The anti-Cx antibodies were raised against synthetic peptides corresponding to the following (intracellular) carboxy-terminal regions: amino acids 315–331 of mouse Cx37 (13), amino acids 335–356 of rat Cx40 (29), amino acids 314–322 of rat Cx43 (17), and amino acids 411–416 of rat Cx46 (40). In some experiments we used mouse monoclonal antibody directed at amino acids 252–270 of rat Cx43 (Transduction), mouse monoclonal anti-desmin antibody (DAKO), or the neurofilament (NF) marker NR4 (DAKO), directed at the 68-kDa component of NFs. Cells were permeabilized with 0.2% Triton X-100 in PBS for 1 h and incubated with 2% BSA in PBS for 30 min and with one of the primary antibodies overnight. Subsequently, cells were incubated with 2% BSA for 30 min and for 2 h with a secondary antibody (goat anti-rabbit or donkey anti-mouse, depending on the primary antibody) labeled with an FITC or Texas red fluorophore. To test for the specificity of immunoreactivity, cells were incubated with a mixture of primary antibody and a 500-fold excess of peptide homologous to the epitope against which the antiserum was directed, or the first antibody was omitted altogether. Immunolabeled tissue sections and isolated cells

were visualized using a Nikon Optiphot-2 microscope equipped for fluorescence microscopy. Images were digitized using a Hitachi HV-C20 charge coupled device camera, and composites were made using Adobe Photoshop 4.0.

Electrophysiology. A symmetrical set-up with two custom-made patch-clamp amplifiers was used. Macroscopic and single-channel recordings were filtered at 2 and 5 kHz and sampled at 1 and 2.5 kHz, respectively. Data were analyzed off-line using MacDaq analysis software (developed by Dr. A. C. G. van Ginneken, Dept. of Physiology, University of Amsterdam, Amsterdam, The Netherlands).

Borosilicate glass patch electrodes were pulled on a Narashige PC-10 puller and fire polished. Electrodes were frontfilled with pipette solution and backfilled with pipette solution containing 0.2 mg/ml amphotericin B (Sigma Chemical). Electrode resistances were between 1 and 4 MΩ. Series resistances were estimated by canceling the fast initial voltage jump in response to a short current injection in the current-clamp mode (42). Within minutes after the cell-attached configuration was attained, series resistances decayed to a steady-state level of 8.2 ± 4.6 MΩ. In voltage-clamp mode, series resistances could be compensated for up to 70% of the value measured in current-clamp mode.

Junctional and membrane currents were measured in the double perforated-patch voltage-clamp mode. Membrane currents of the individual cells forming a pair were measured by stepping both cells simultaneously to the same potential from a common holding potential of −40 mV. On a step in potential in one cell of a pair, junctional current was recorded in the other cell.

The total resistance (the recorded junctional current divided by the applied potential difference) is the sum of the junctional resistance and the uncompensated parts of the series resistances. Uncompensated series resistance, i.e., the difference between the series resistances measured in current-clamp mode and the series resistances compensated in voltage-clamp mode, would have caused a systematic error in an estimate of G_j (42). To eliminate this error, records were corrected subsequently by subtracting uncompensated series resistances from the total resistance to yield the true junctional resistance. For G_j-V_j relations, the expected voltage drops over the uncompensated series resistances were subtracted from the applied potential difference to yield the true V_j.

Gating of single gap junction channels could be observed after partial uncoupling with halothane. Periods with numerous multiple states were excluded from the analysis, and only transitions from the baseline to a full open state were analyzed. Single-channel conductance histograms were fitted in KaleidaGraph (Adelbeck Software) with one, two, or three Gaussian distributions using the least-squares method. Values are means ± SD.

Spontaneous electrical activity was recorded in the double perforated-patch current-clamp mode. All electrophysiological recordings were performed at 35°C, under continuous perfusion with normal modified Tyrode solution.

Composition of salines was as follows: Pipette solution contained (in mmol/l) 125 potassium gluconate, 10 KCl, 2 $MgCl_2$, 0.6 $CaCl_2$, 4 Na_2ATP, 5 EGTA, and 5 HEPES, with pCa 7.6 and pH adjusted to 7.2 with KOH. Amphotericin B was stored as a 60 mg/ml stock solution in DMSO at −20°C for ≤6 h. Pipette solution containing 0.2 mg/ml amphotericin B was stored in the dark for up to 1 h.

RESULTS

Cx expression in the SA node. On the basis of microelectrode mapping studies in the rabbit SA node, the dominant pacemaker is expected to be located at ~3 mm from the superior vena cava (4). From this region, we have cut serial sections to analyze Cx expression. In the rabbit, the SA node can be distinguished from the adjacent atrium by its immunoreactivity to NF marker (Fig. 1, *D* and *G* vs. *E, F, H*, and *I*) (19, 48). In addition, the pattern of anti-desmin labeling in the SA node differed markedly from that in the atrium. In the atrial myocardium, anti-desmin labeling clearly revealed the cross-striation of the myocytes and more intense labeling in intercalated disks (Fig. 1*A*). In the SA node, labeling was more uniform and overall more intense (Fig. 1, *B* and *C*). We have used both antibodies as markers for the nodal area in double-labeling experiments with anti-Cx37, anti-Cx40, anti-Cx43, anti-Cx45, and anti-Cx46 antibodies. As expected (50), endothelial cells in atrial blood vessels reacted with anti-Cx37 and anti-Cx40 antibody (not shown). Anti-Cx40, anti-Cx43, anti-Cx45, and anti-Cx46 exhibited immunoreactivity in the SA node, the pattern of which we have analyzed in detail (Fig. 1). The anti-Cx40, anti-Cx43, and anti-Cx46 antibodies that were raised in rabbit displayed vague background fluorescence in the nodal area. This background was not reduced by coincubation with peptides homologous to the epitopes against which these antibodies were raised and is, therefore, nonspecific.

Cx40 was detected in the atrial myocardium (Fig. 1*A*). In the central part of the SA node, anti-Cx40 immunoreactivity could also be observed (Fig. 1*C*). However, immunofluorescence in this area consisted of small, faint spots of anti-Cx40 labeling, rather than the larger spots present between atrial myocytes, suggesting that gap junctions in the SA node are smaller and represent less of the total contact area between cells.

Immunoreactivity to rabbit polyclonal anti-Cx43 was observed throughout the atrium (Fig. 1*D*). In the NF marker-positive cells of the central portion of the SA node, however, no binding of anti-Cx43 antibody could be detected (Fig. 1*F*). Interestingly, on the interface between atrium and SA node, anti-Cx43 immunoreactivity was observed in strands of cells that were positive for NF marker (Fig. 1*E*) and showed intense anti-desmin labeling, typical of SA node myocytes.

Within the SA node, anti-Cx46 immunoreactivity showed the same pattern as anti-Cx40 immunoreactivity. It was also present in small spots in NF marker-positive cells, with the typical anti-desmin staining pattern (Fig. 1*I*). However, anti-Cx46 immunoreactivity could not be detected in the atrial myocardium (Fig. 1*G*).

Punctate, brilliant labeling by anti-Cx40 and anti-Cx46 antibodies was abolished by an excess of peptides homologous to the epitopes against which they were directed (not shown) and was, therefore, specific. In contrast, background fluorescence was unaffected by coincubation with these peptides and was probably due

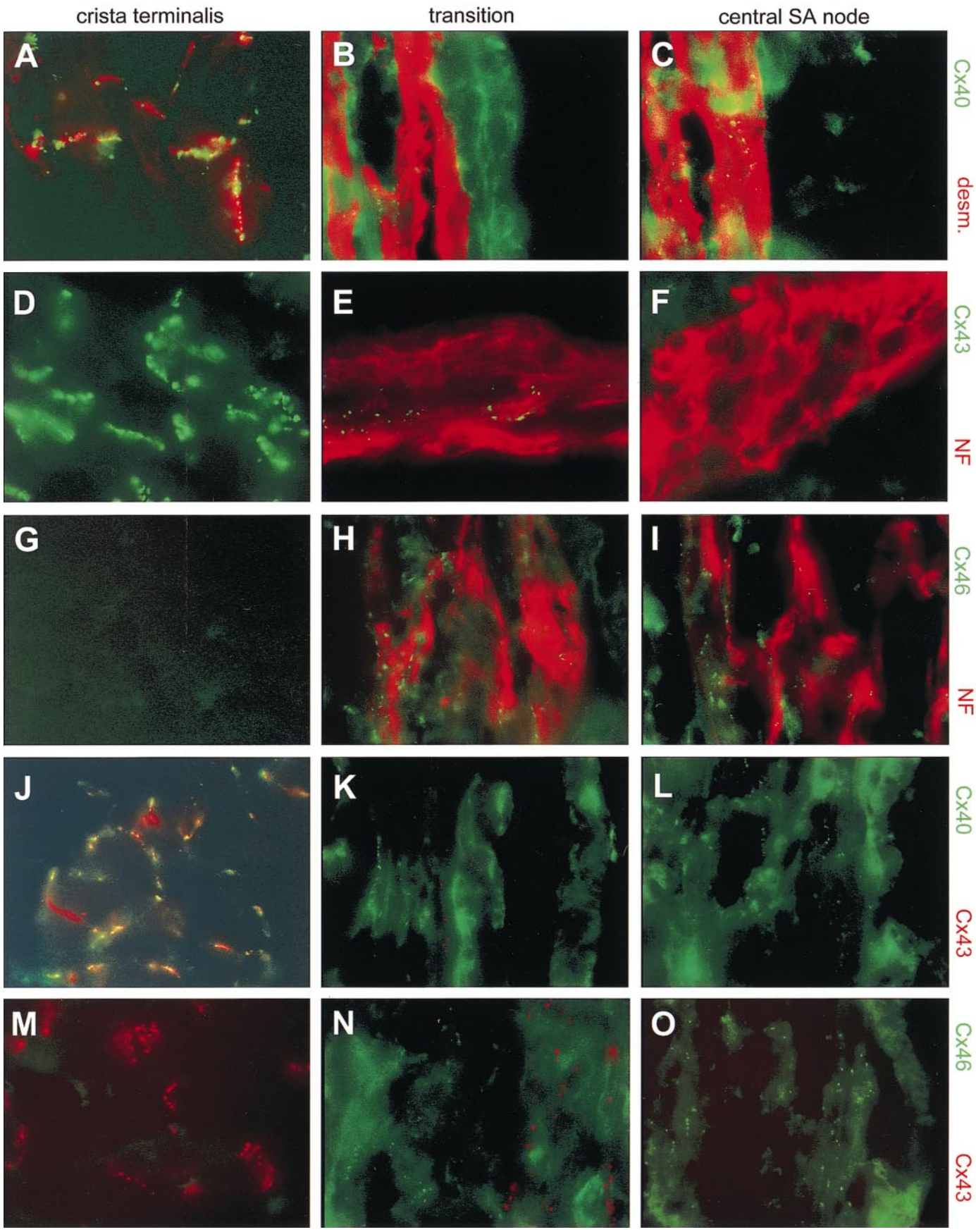

to nonspecific binding of the goat anti-rabbit secondary antibody in rabbit tissue.

From Fig. 1, *B, E,* and *H*, it is apparent that, in the area between the crista terminalis and the central SA node, Cx40, Cx43, and Cx46 were detectable in some, but not all, groups of cells.

To compare expression patterns of Cx40 and Cx46, on the one hand, and Cx43, on the other, we performed double-labeling experiments with mouse monoclonal anti-Cx43 and either anti-Cx40 or -Cx46. In the right atrium, labeling with anti-Cx40 and anti-Cx43 showed some overlap (yellow color in Fig. 1*J*). This overlap was less complete than that observed in the bulk atrial myocardium (50): in the atrial myocardium close to the crista terminalis, Cx40 was less abundant than Cx43 (red color in Fig. 1*J*). In the transitional area between the right atrium and the SA node, cells in Cx43-positive strands showed no detectable immunostaining with anti-Cx40 antibody (Fig. 1*K*) or anti-Cx46 antibody (Fig. 1*N*). However, Cx40 or Cx46 could be detected in adjacent Cx43-negative strands (Fig. 1, *K* and *N*, respectively). Toward the right atrium, the relative abundance of anti-Cx43 labeling increased, whereas Cx40 and Cx46 immunoreactivity decreased: in NF marker-positive tissue immediately adjacent to the crista terminalis, only Cx43 could be detected (not shown).

Cx expression in isolated myocytes from the SA node. Isolated cells from the region of the SA node displayed a large variability in morphology, ranging from cells indistinguishable from typical atrial myocytes to the "spider," "spindle," and "elongated spindle" cells, which have been shown to possess pacemaker properties (48). Not all pacemaker myocytes were immunoreactive to NF marker, but in the area of the SA node, only pacemaker myocytes label with this marker (48). Most spindle and spider cells showed labeling with NF marker or intense uniform labeling with anti-desmin antibody. Many elongated spindle cells showed NF marker immunoreactivity and intense anti-desmin labeling with a clearer cross-striated pattern than spider and spindle cells. Cells with the morphology of atrial myocytes were not immunoreactive to NF marker and showed a pronounced cross-striated pattern of anti-desmin labeling. Cx40, Cx43, and Cx46 were expressed in subgroups in the isolate. Anti-Cx40 and anti-Cx43 labeling was observed in anti-NF-negative cells with a typical atrial morphology (Fig. 2, *A* and *D*), whereas anti-Cx46 labeling could not be detected in these cells (Fig. 2*G*).

In spindle and spider cells that were NF marker-positive or showed the intense anti-desmin staining, the Cx expression pattern was strikingly different from that in atrial myocytes. Many of these putative pacemaker myocytes labeled with anti-Cx40 (Fig. 2*C*) or anti-Cx46 (Fig. 2*I*). The pattern of Cx40 and Cx46 immunoreactivity in spindle and spider cells comprised small, faint spots distributed over the cell surface, including the processes, rather than the much larger, more conspicuous patches of labeling observed between atrial myocytes. Typically, NF marker-positive cells with the morphology of elongated spindle cells showed staining with anti-Cx43 (Fig. 2*E*), but not with anti-Cx40 and anti-Cx46 (Fig. 2, *B* and *H*).

To investigate whether cells labeled with anti-Cx40, anti-Cx43, or anti-Cx46 represent separate populations, we performed double-labeling experiments with anti-Cx40 or anti-Cx46 antibody and mouse monoclonal anti-Cx43 antibody (Fig. 2, *J–O*). In tissue sections, the expression pattern observed with this mouse anti-Cx43 antibody did not differ from that observed with the rabbit polyclonal antibody. The diffuse green background visible in Fig. 2, *J–O*, was also observed when the primary antibody was omitted. In addition, this background level was not reduced by coincubation during the primary antibody step with peptides homologous to the epitopes against which the primary antibodies were raised. Therefore, this background fluorescence does not represent specific binding to Cx proteins. Most cells with an atrial morphology expressed Cx40 and Cx43 (Fig. 2*J*). In this Cx43-expressing cell type, Cx46 was not detectable (Fig. 2*M*). In the cells in Fig. 2, *K* and *N*, Cx43, but not Cx40 or Cx46, could be detected. These cells might represent elongated spindle cells, but because of the variability in cell morphology, it is difficult to make an absolute distinction between elongated spindle cells and atrial myocytes without confirmation from anti-desmin or NF marker labeling. Typically, spindle and spider cells expressed Cx40 and/or Cx46 (Fig. 2, *L* and *O*). Only in very few of the cells with a typical morphology of pacemaker myocytes that were anti-Cx46 or anti-Cx40 positive, could expression of anti-Cx43 be detected, suggesting that there is only a small overlap between the population expressing Cx43 and the population expressing Cx40 and/or Cx46.

Macroscopic G_j. Because of our interest in electrical coupling between pacemaker cells, we recorded from pairs of spindle or spider cells, which often displayed weak spontaneous contractions and had only faint cross-striation. All experiments were performed at 35°C using the perforated-patch method to prevent washout of cytoplasmic constituents. A representative recording from a pacemaker myocyte from the SA node is shown in Fig. 3, indicating the criteria we have used to recognize true pacemaker cells. In current-clamp mode, this cell fired action potentials spontaneously, as expected for a pacemaker myocyte (Fig. 3*A*). Membrane resistances were ≥250 MΩ. In response to a simultaneous step to negative potentials in both cells

Fig. 1. Connexin (Cx) expression in tissue sections from the sinoatrial (SA) node. *A, D, G, J*, and *M*: right atrial myocardium near the crista terminalis; *B, E, H, K*, and *N*: transitional area between the central SA node and the crista terminalis; *C, F, I, L*, and *O*: central SA node. *A–C*: anti-desmin (red) and anti-Cx40 (green); *D–F*: neurofilament (NF) marker (red) and anti-Cx43 (green); *G–I*: NF marker (red) and anti-Cx46 (green). *J–L*: anti-Cx43 (red) and anti-Cx40 (green); *M–O*: anti-Cx43 (red) and anti-Cx46 (green). Magnification ×600.

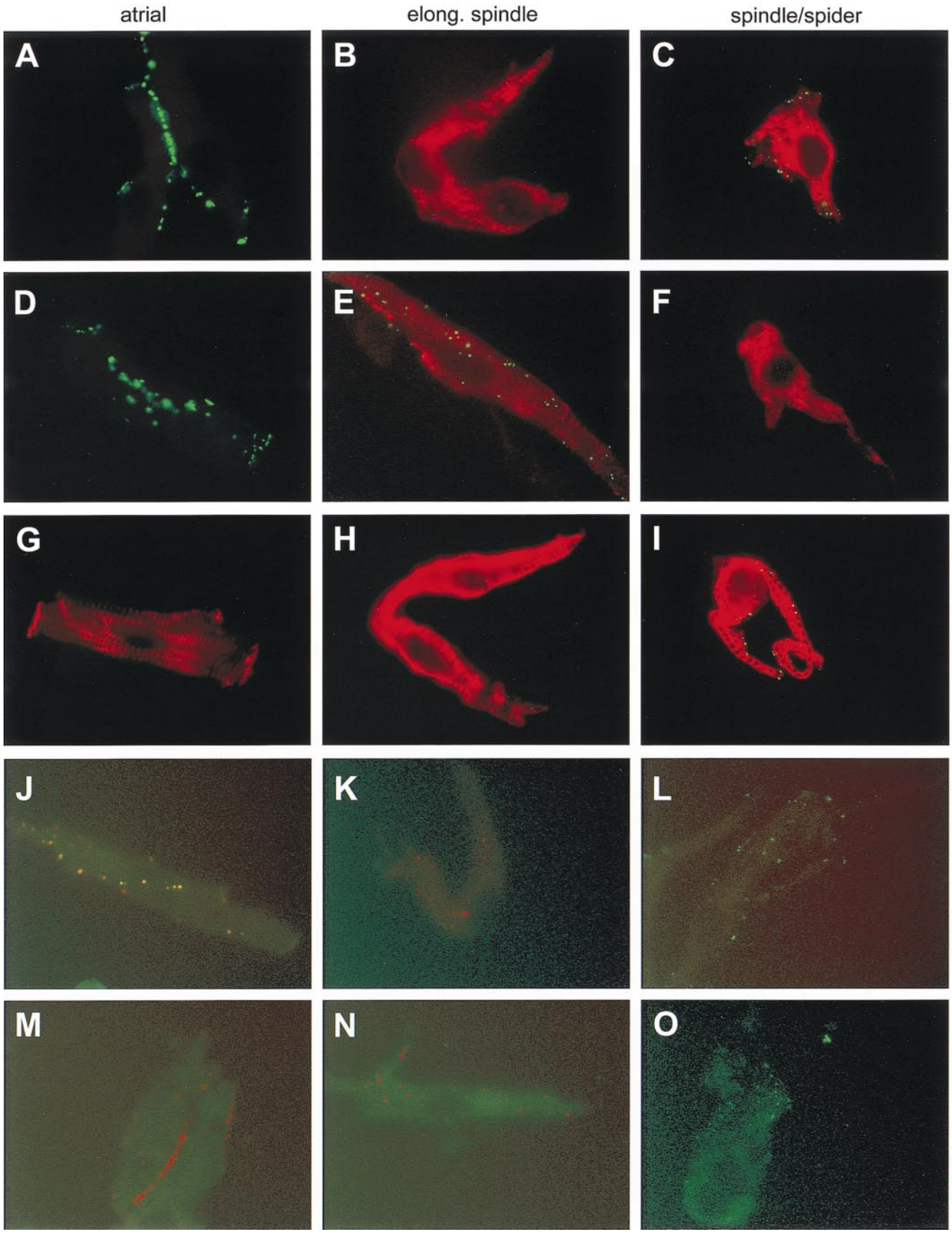

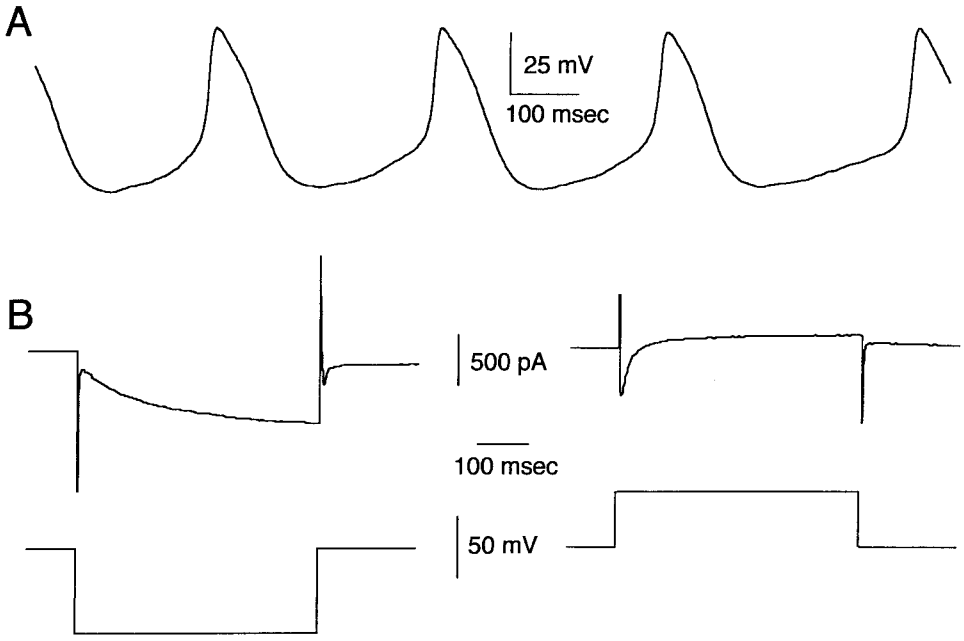

Fig. 3. Electrophysiological properties of a single pacemaker myocyte. *A*: spontaneous action potential recorded in the current-clamp mode. *B*, *left*: during a hyperpolarizing step from a holding potential of −40 to −100 mV (*bottom trace*), the slow activation of an inward current (I_f) was observed (*top trace*). *B, right*: depolarizing step from −40 to 0 mV (*bottom trace*) evoked a transient inward current ($I_{Ca,L}$, *top trace*).

from a holding potential of −40 mV, the slow activation of hyperpolarizing-activated current (I_f) is apparent, which is characteristic for pacemaker myocytes from the SA node (15). On depolarizing steps from −40 mV, L-type Ca^{2+} current was activated (Fig. 3*B*).

Recordings were made on pairs of connected cells. During a step in potential in one cell, junctional current could be observed in the other. For a total of 36 pairs, the values for the macroscopic G_j, which have been corrected for series resistance, are represented in the histogram in Fig. 4. This yields a skewed distribution, with a mean of 7.5 ± 6.4 nS and a median of 5.3 nS.

Sensitivity of G_j to V_j. For most types of gap junctions, junctional current decays during sustained large V_js. We have evaluated the voltage sensitivity of gap junctions in pairs of SA node myocytes by applying steps in potential ranging from −100 to +100 mV during 4 s, from a common holding potential of 0 mV. A representative example of junctional current traces and a G_j-Vj relation is shown in Fig. 5*A*. Even at a V_j of +100 or −100 mV, there was only a moderate decay of the junctional current. This is reflected in Fig. 5*A*, *right*, where the average instantaneous and steady-state normalized G_j values are plotted against V_j.

An example of a recording from a pair with a relatively low macroscopic G_j is shown in Fig. 5*B, left*. Here, the junctional resistance (0.9 GΩ) was high compared with the series resistances (6 and 8 MΩ) and membrane resistances (both ~0.5 GΩ). Even under these favorable recording conditions, there was a decay of the junctional current of only 20% during a 4-s step to 100 mV.

In this pair, it was possible to resolve single-channel events without chemical uncoupling. Although this recording had a poor signal-to-noise ratio, gating from a channel type with a large single-channel conductance of ~200 pS was observed (Fig. 5*B, right*).

Single gap junction channel conductances. In a number of pairs with a morphology typical of pacemaker myocytes, which exhibited spontaneous action potentials in the current-clamp mode, in which I_f could be activated in the voltage-clamp mode, and in which the G_j showed only moderate V_j sensitivity, we used halothane to lower the open probability of gap junction channels to record single-channel events with greater accuracy (Fig. 6*A*). In each of these recordings, several populations of unitary current amplitudes were present, but in slightly different proportions. Data from five experiments were pooled and are represented in the conductance histogram in Fig. 6*B*. This histogram was best fit with a sum of three Gaussian distributions, with peaks at 133, 202, and 241 pS.

Synchronization in pacemaker cell pairs. If both cells in a pair are stepped to the same potential from a common holding potential, there will be no V_j and, consequently, no net current will flow across the junction. With the use of this protocol, current-voltage relations of the membranes of both cells could be recorded simultaneously. As exemplified in Fig. 7*A*, the membrane currents in the two cells within a pair will show small differences in current amplitudes. These

Fig. 2. Cx expression in myocytes isolated from the SA node. *A, D*, and *G*: atrial myocytes; *B, E*, and *H*: elongated spindle cells; *C, F*, and *I*: spider/spindle cells. *A–C*: NF marker (red) and anti-Cx40 (green); *D–F*: NF marker (red) and anti-Cx43 (green); *G–I*: anti-desmin (red) and anti-Cx46 (green). *J–L*: anti-Cx43 (red) and anti-Cx40 (green); *M–O*: anti-Cx43 (red) and anti-Cx46 (green). Magnification ×600.

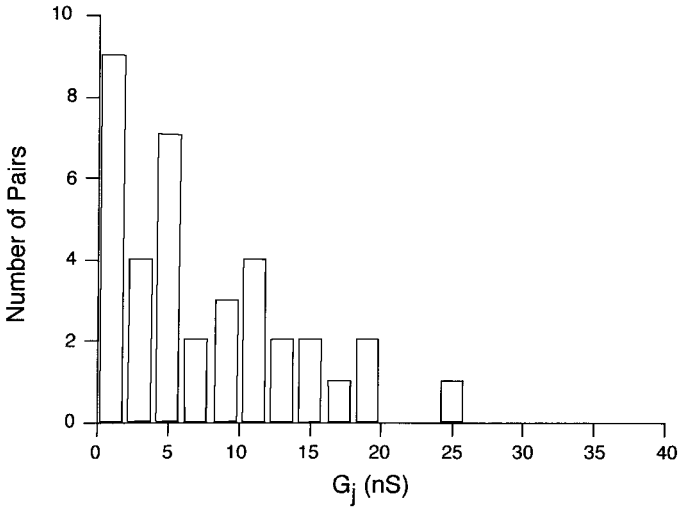

Fig. 4. Macroscopic junctional conductance (G_j) in pairs of pacemaker myocytes. Frequency histogram of macroscopic G_j, corrected for series resistance, in a total of 36 cell pairs. Values ranged from 0.6 to 25.0 nS with an average of 7.5 ± 6.4 nS and a median of 5.3 nS.

differences, together with the difference in membrane capacitance, would lead to a difference in beating frequency in unconnected cells. However, these cells were connected by a macroscopic G_j of 6.2 nS, and synchronous action potentials were recorded from this pair in current-clamp mode and are shown superimposed in Fig. 7*B, top trace*. For an ohmic junctional resistor, the junctional current is expected to be equal to the difference in membrane potential divided by the junctional resistance. The difference in potential is plotted in Fig. 7*B, bottom trace*. During the upstroke of the action potential, depolarizing current flows from the inherently faster-beating cell to the inherently slower-beating cell, whereas during repolarization, depolarizing current flows from the slower- to the faster-beating cell.

Figure 7*C* depicts action potentials in a pair with a relatively small macroscopic G_j of 0.66 nS. This pair showed a less complete waveform entrainment than the pair in Fig. 7*B*, and the maximal junctional current during the upstroke will have been smaller. Nevertheless, this current was sufficient to synchronize the two pacemaker myocytes.

DISCUSSION

Cx distribution in the rabbit SA node. We have studied Cx expression in transverse sections from the rabbit SA node. Labeling patterns of NF marker (19, 48) and anti-desmin were used to delineate the SA node.

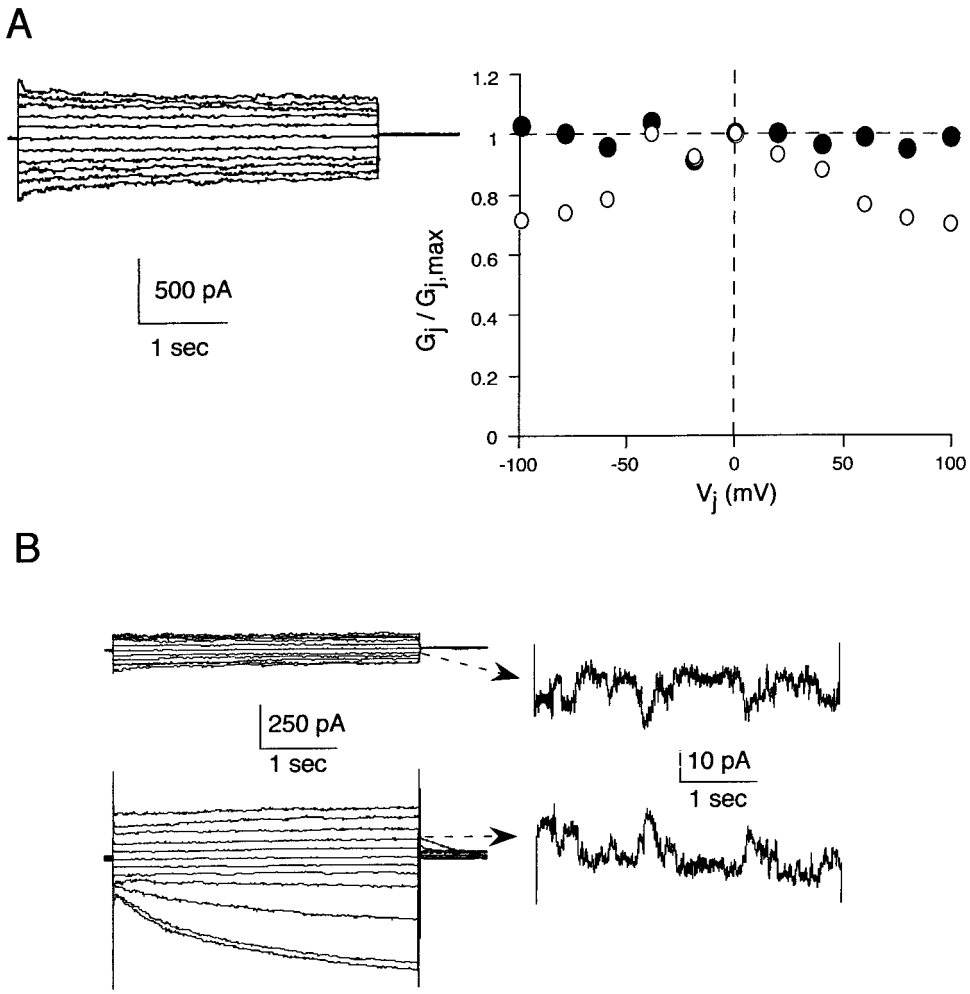

Fig. 5. Sensitivity of G_j to the transjunctional potential difference (V_j). *A*: moderate sensitivity to V_j. *Left*: junctional current during 4-s steps in potential ranging from −100 to +100 mV from a common holding potential of 0 mV. *Right*: instantaneous (●) and steady-state (○) normalized G_j-V_j relations of this cell pair. V_j values have been corrected for the voltage drops over the uncompensated part of the series resistances. *B*: poorly coupled cell pair: currents in the nonstepped cell (*top left*) and stepped cell (*bottom left*) during steps in potential ranging from −100 to +100 mV from a common holding potential of 0 mV. *Right*: unitary events of ~200 pS can be resolved on an expanded scale, V_j = 40 mV. In both cell pairs, membrane resistances were 400–500 MΩ.

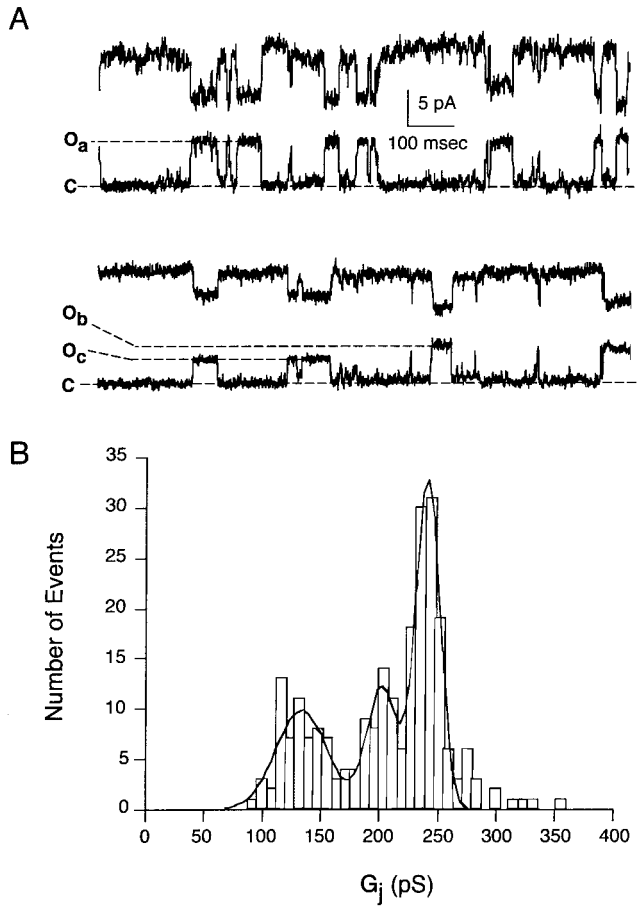

Fig. 6. Single gap junction channel conductances in pacemaker myocyte pairs. *A*: single-channel activity at V_j = 25 mV. C, closed level. *Top traces*: transitions of a channel with a unitary conductance of ~250 pS (O_a). *Bottom traces*: transitions of channels with amplitudes O_b and O_c, corresponding to single-channel conductances of ~200 and 130 pS, respectively. *B*: pooled single-channel conductance histogram from 5 separate recordings on pacemaker myocyte pairs. The histogram was best fit as the sum of 3 Gaussian distributions with means of 133 ± 31, 202 ± 18, and 241 ± 15 pS.

As expected, Cx40 and Cx43 are expressed in the myocardium adjoining the SA node (50), although expression of Cx40 is less abundant in the bulk atrial myocardium. In the NF marker-positive central nodal area, Cx40 and Cx46 were detected. In agreement with the poor electrical coupling, immunofluorescent spots in the central node were small and faint compared with those in the atrial myocardium. Interestingly, fibers that were positive to NF marker and anti-Cx43 were observed in the area between the crista terminalis and the central SA node. These anti-Cx43-positive fibers, in which Cx40 and Cx46 could not be detected, ran alongside fibers probably expressing Cx40 and Cx46, although colocalization of Cx40 and Cx46 could not be confirmed directly, because both antibodies were raised in rabbit. Boundaries between Cx43- and Cx40/Cx46-expressing strands were sharp. Strands of myocytes expressing Cx43 have been observed in guinea pig (47) and dog (31) SA nodes. In the guinea pig, anti-α-smooth muscle actin (anti-α-SMA) specifically labeled pacemaker myocytes, but not atrial myocytes. In the transitional area, anti-Cx43 and anti-α-SMA showed complementary labeling in separate strands. On the basis of these observations, ten Velde et al. (47) concluded that the atrium forms interdigitations into the nodal area. In the rabbit, anti-α-SMA did not label pacemaker tissue specifically (not shown). However, in our double-labeling experiments, Cx43-positive strands labeled with anti-desmin and NF marker in a pattern similar to pacemaker myocytes, rather than atrial myocytes. These results therefore suggest that the Cx43-expressing strands in rabbit consist of transitional cells. The difference in the nature of these strands might reflect structural differences between guinea pig and rabbit SA nodes. Interestingly, sharp transitions in action potential morphology over small distances have been encountered in the guinea pig, but not in the rabbit (39). In the anti-Cx43-positive strands in the rabbit, no anti-Cx40 immunoreactivity could be detected. Expression of Cx40 was not analyzed in the guinea pig SA node, but in the dog the anti-Cx43-positive strands also expressed Cx40. In all three cases, the observed anti-Cx43-positive strands may function as preferential conduction pathways from the central node to the atrium. In addition, they might provide a gradual increase in cell-to-cell coupling from the central node toward the right atrium, which, in modeling studies, prevents clamping of the small SA node to the relatively negative resting potential of the atrium (26).

Recently, Coppen et al. (11) described the distribution of Cx40, Cx43, and Cx45 in the rabbit SA node, studied by immunohistochemistry combined with confocal microscopy. These authors report that Cx40 and Cx45 are expressed in the central SA node, whereas Cx43 is expressed in the crista terminalis. Unlike Cx40 (11; this study) and Cx46 (this study), Cx45 was coexpressed with Cx43 in a restricted zone at the nodal-crista terminalis border (11). Coppen et al. also described the presence of bundles expressing Cx43, which were referred to as penetrating bundles of atrial myocytes. Our observations in double-labeling experiments with anti-desmin and NF marker suggest that these bundles consist of transitional pacemaker cells, rather than atrial myocytes.

Cx expression in isolated myocytes from the SA node. The complexity in morphology and Cx expression observed in tissue sections was reflected in the diversity observed in isolated cells. We used NF marker to distinguish pacemaker myocytes. Not all pacemaker myocytes are positive to this marker, but positive cells have been shown to represent pacemaker myocytes (48). Most spindle and spider cells, which were positive to NF marker and labeled strongly and uniformly with anti-desmin, were immunoreactive to Cx40 and/or Cx46. Immunoreactivity to anti-Cx43 and NF marker was observed mainly in elongated spindle cells, which have been suggested to represent transitional cells (48). Colocalization of Cx40 and Cx43 was often observed in cells with the morphology of atrial myocytes and only rarely in spider, spindle, and elongated spin-

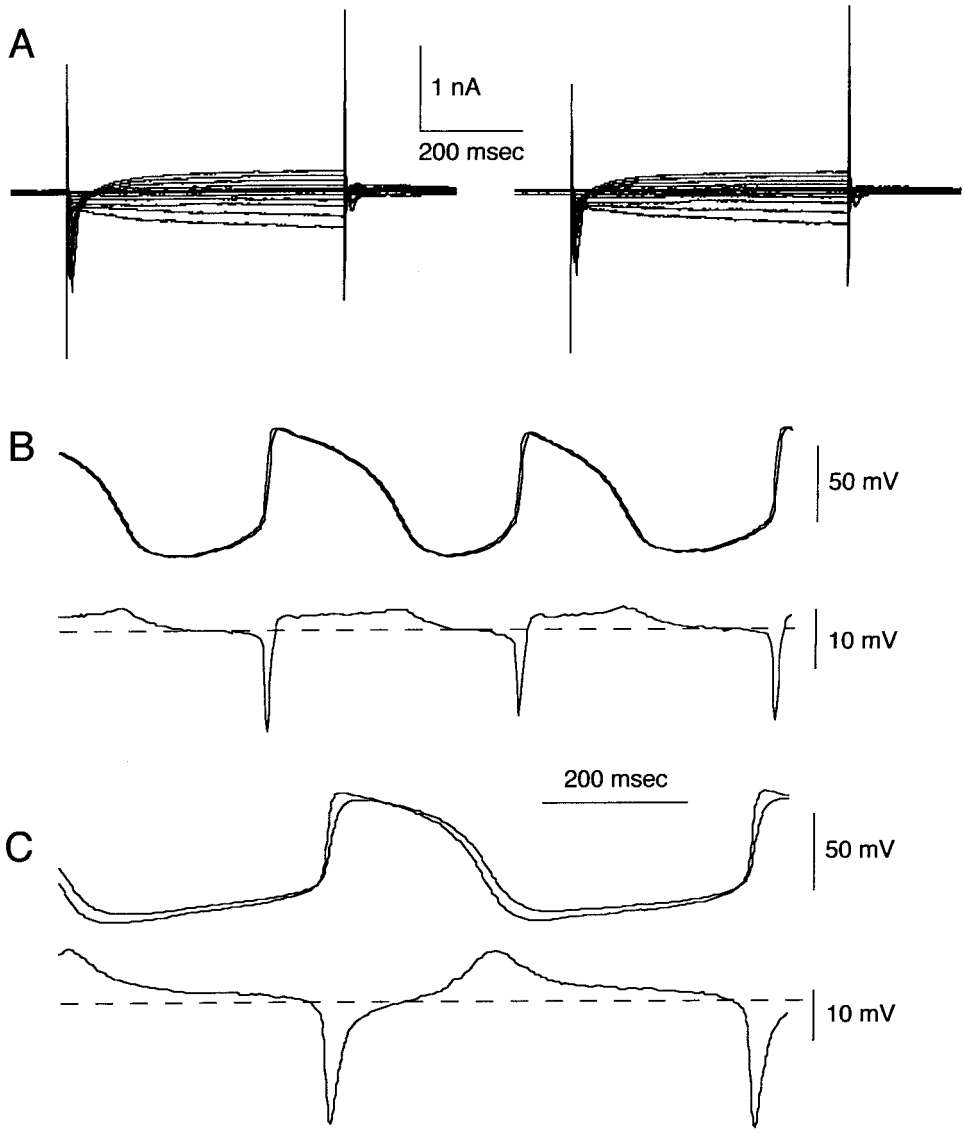

Fig. 7. Synchronicity in pacemaker myocyte pairs. *A*: membrane currents elicited by simultaneous 500-ms steps to potentials ranging from −100 to + 30 mV from a common holding potential of −40 mV in 2 cells connected by a junctional conductance of 6.2 nS. *B*, *top traces*: superimposition of synchronous action potentials recorded from the same pair in current-clamp mode; *bottom trace*: difference in membrane potential between the 2 cells, corresponding to the flow of current that synchronizes the 2 pacemaker myocytes. Dashed line, voltage difference of 0 mV. The voltage difference represented by the horizontal scale bar corresponds to a junctional current of 62 pA. *C*, *top traces*: superimposed action potential from a cell pair with G_j = 0.66 nS; *bottom trace*: difference in membrane potential. Scale bar corresponds to a junctional current of 6.7 pA.

dle cells. Similarly, colocalization of Cx43 and Cx46 in these cells was rare.

Electrophysiological recordings on pacemaker myocyte pairs. In addition to this immunohistochemical and immunocytochemical characterization of Cx expression, we have recorded from cell pairs from the area of the SA node. In a study describing similar recordings on cells from the rabbit SA node, Anumonwo et al. (1) demonstrated the presence of Cx43 in cell pairs with immunocytochemical methods. In recordings from these pairs, the single-channel conductance histogram and the sensitivity of the G_j to V_j were in agreement with the properties of Cx43. Although the average macroscopic G_j we have measured is similar, the G_j-V_j relation and single-channel conductances are clearly different. Moreover, we could not detect Cx43 in the central area of the rabbit SA node. Importantly, we have used criteria for recognizing pacemaker myocytes that are different from those used by Anumonwo et al. Whereas these authors recorded preferentially from round cells with high input resistance, we have recorded from spider and spindle cells, which are believed to represent true pacemaker myocytes by many authors studying isolated cells from the SA node (14, 15, 21, 48). In addition to recording spontaneous action potentials in current-clamp mode, we have routinely checked in voltage-clamp mode for the presence of I_f, which is characteristic of pacemaker myocytes (15). We are, therefore, confident that we have recorded from true pacemaker myocytes. These criteria were used to select pacemaker myocytes in our double whole cell recordings. For this reason, our electrophysiological data do not reflect the diversity of cell types and Cx expression observed in our immunocytochemical experiments.

After correction for series resistance, the average macroscopic G_j in pacemaker myocyte pairs was 7.5 nS, which is more than an order of magnitude lower than the values we previously reported for myocyte pairs from the rabbit atrial and ventricular working myocar-

dium (50). This poor electrical coupling agrees with observations that gap junctional plaques in the SA node are small and sparse compared with those in the working myocardium (32) and might contribute to the relatively low conduction velocity measured in the rabbit SA node (9, 30).

The sensitivity of the G_j to V_j was only very moderate in pacemaker myocyte pairs from the SA node. In double whole cell voltage-clamp recordings, the sensitivity to V_j can be obscured by voltage drops across series resistances (54). For a number of reasons, we believe that the moderate V_j sensitivity observed by us in typical pacemaker myocyte pairs is not artifactual. First, in our perforated-patch recordings, junctional resistances (40 MΩ to 1.6 GΩ) were high compared with average series resistances [8.2 ± 4.6 MΩ, close to the value obtained by Habuchi et al. (22) using a similar method]. Moreover, comparable G_j-V_j relations were obtained in standard double whole cell recordings with potassium gluconate as charge carrier (not shown). Second, the Ca^{2+} current was well clamped under our recording conditions, indicating adequate voltage control. Third, the moderate V_j sensitivity was also observed in cell pairs that were very poorly coupled and in which single channels could be resolved without chemical uncoupling (Fig. 5*B*). Model studies have shown that V_j sensitivity is also decreased if gap junction channels are assembled in large plaques (54). However, gap-junctional plaques in pacemaker cells are relatively small (32), and therefore it is unlikely that this effect can explain the shape of the steady-state G_j-V_j relation typical of pacemaker myocyte pairs.

Published values for half-maximal potential and minimum conductance range from 15 mV and 0.1 for Cx45 (34), 50 mV and 0.3 for Cx40 (8), and 60 mV and 0.4 for Cx43 (35) to 67 mV and 0.1 for Cx46 (52). Thus the observed sensitivity to V_j in pacemaker myocyte pairs is smaller than that of any of the Cx types detected in the SA node (11; this study). A number of recent studies have investigated the properties of gap junctions in cells coexpressing two types of Cx (3, 6, 16, 24). In all cases where electrophysiological properties of putative heteromeric channels were explored, V_j sensitivity was found to be reduced compared with homomeric channels formed by the constituent Cxs (6, 16, 24). Although we do not possess the means to investigate this directly, the observed small sensitivity to V_j might be due to the occurrence of heteromeric channels in pacemaker cells of the SA node. With their modest sensitivity to V_j, these gap junctions will behave as simple ohmic conductors in the intact tissue.

From pacemaker myocyte pairs, we obtained single-channel conductance histograms with main populations at 133, 202, and 241 pS. If single-channel conductances recorded using the perforated-patch method are comparable to those measured using potassium gluconate as charge carrier, this is not compatible with the elongated spindle cell population expressing predominantly Cx43, because Cx43 is expected to have single-channel conductance of 20, 40–45, and 70 pS in potassium gluconate (43). In addition, from their morphology, it is highly probable that these pairs correspond to the pacemaker myocyte population expressing Cx40 and Cx46. On the basis of observations reported by Coppen et al. (11), it is likely that these myocytes also express Cx45. It is not straightforward to link the observed single-channel conductances with these Cxs, especially since they might form heteromeric gap junction channels. For human Cx45, a single-channel conductance of 20 pS in KCl has been reported (34). Given the signal-to-noise ratio in our experiments, channels formed by Cx45 will probably have escaped detection. Unitary conductances of 121 and 153 pS for mouse Cx40 in KCl (45) and 158 pS for rat Cx40 in potassium glutamate (2) have been reported. To our knowledge, no reports have been published on the single-channel conductance of Cx46, but the reported unitary conductance of rat Cx46 hemichannels is 300 pS (46). If the unitary conductance of the complete channel were simply equal to that of two hemichannels in series, it would be 150 pS, similar to the unitary conductance of channels formed by Cx40. The peak at 133 pS could therefore represent gating of channels formed by Cx40 or Cx46. It is unlikely that the populations at 202 and 241 pS can be ascribed to gating of channels formed by Cx40, but neither can they be ascribed to Cx46 with any certainty. Nonetheless, the single-channel conductance histogram from pacemaker myocyte pairs clearly differs from that obtained in rabbit atrial and ventricular myocytes (50), indicating the presence of at least one channel type not present in the working myocardium, which, from our immunocytochemical data, is likely to be Cx46.

Our results do not allow us to infer relative contributions of Cx subtypes or main single-channel conductances to the macroscopic G_j. There are nevertheless some implications with respect to electrical coupling between pacemaker cells. Combined modeling and experimental studies have shown that pacemaker myocytes from the SA node require a minimal coupling conductance on the order of 0.1 nS for synchronization (49, 56). Therefore, one single channel with any of the unitary conductances observed by us would be sufficient to synchronize two cells. Moreover, only 20–40 open channels are sufficient for the observed medial macroscopic conductance of 5.3 nS.

For a number of types of Cx, the ability to pair with other types of Cx has been investigated in *Xenopus* oocytes (for review see Ref. 7). In *Xenopus* oocytes, Cx40 hemichannels do not form functional gap junction channels with Cx43 or Cx46 hemichannels, whereas Cx43 can form heterotypic channels with Cx46 (53). Cx45, which has also been detected in the central SA node (11), can form heterotypic channels with Cx40 and Cx43. Whether incompatibility of Cx can affect electrical coupling in the SA node is complicated by recent observations that Cx40 and Cx43, which cannot form heterotypic channels in *Xenopus* oocytes, may form heteromeric channels when coexpressed with one cell (24).

Several studies indicate that, compared with hemichannels formed by other Cxs, Cx46 hemichan-

nels are more prone to open on membrane depolarization (40, 46). The high membrane resistance of pacemaker myocytes would be significantly affected by opening of such large-conductance hemichannels, but we are not aware of any studies on SA node pacemaker myocytes describing membrane channels that resemble the Cx46 hemichannels in behavior.

This report is one of the first to describe the biophysical properties of gap junctions in the SA node at the level of pacemaker myocyte pairs. Double whole cell recording will also enable the study of regulation of these gap junctions in the SA node. Whereas the effects of many agents on membrane channels in the SA node have been studied in detail in isolated cells, regulation of gap junction channels has received comparatively little attention. In the working myocardium, where intercellular and membrane resistances are low, it is questionable whether moderate changes in G_j would significantly affect conduction. In nodal tissue, however, with poor electrical coupling and high membrane resistances, even small changes in G_j might have profound effects on conduction and synchronization.

The authors acknowledge Dr. Ronald Wilders for stimulating discussions.

REFERENCES

1. **Anumonwo JMB, Wang H-Z, Trabna-Janik E, Dunham B, Veenstra RD, Delmar M, and Jalife J.** Gap junction channels in adult mammalian sinus nodal cells: immunolocalization and electrophysiology. *Circ Res* 71: 229–239, 1992.
2. **Beblo DA, Wang H-Z, Beyer EC, Westphale EM, and Veenstra RD.** Unique conductance, gating, and selective permeability properties of gap junction channels formed by connexin40. *Circ Res* 77: 813–822, 1995.
3. **Bevans CG and Harris AL.** Direct high-affinity modulation of connexin channel activity by cyclic nucleotides. *J Biol Chem* 274: 3720–3725, 1999.
4. **Bleeker WK, Mackaay AJC, Masson-Pévet M, Bouman LN, and Becker AE.** Functional and morphological organization of the rabbit sinus node. *Circ Res* 46: 11–22, 1980.
5. **Bouman LN, Duivenvoorden JJ, Bukauskas FF, and Jongsma HJ.** Anisotropy of electrotonus in the sinoatrial node of the rabbit heart. *J Mol Cell Cardiol* 21: 407–418, 1995.
6. **Brink PR, Cronin K, Banach K, Peterson E, Westphale EM, Seul KH, Ramanan SV, and Beyer EC.** Evidence for heteromeric gap junction channels formed from rat connexin43 and human connexin37. *Am J Physiol Cell Physiol* 273: C1386–C1396, 1997.
7. **Bruzzone R, White TW, and Paul DL.** Connections with connexins: the molecular basis of direct intercellular signalling. *Eur J Biochem* 238: 1–27, 1996.
8. **Bukauskas FF, Elfgang C, Willecke K, and Weingart R.** Biophysical properties of gap junction channels formed by mouse connexin40 in induced pairs of transfected human HeLa cells. *Biophys J* 68: 2289–2298, 1995.
9. **Bukauskas FF, Veteikis RP, Gotman AM, and Mutskus KS.** Intercellular coupling in the sinus node of the rabbit heart. *Biofizika* 22: 108–112, 1977.
10. **Coppen SR, Dupont E, Rothery S, and Severs NJ.** Connexin45 expression is preferentially associated with the ventricular conduction system in mouse and rat heart. *Circ Res* 82: 232–243, 1998.
11. **Coppen SR, Kodama I, Boyett MR, Dobrzynski H, Takagisji Y, Honjo H, Yeh H-I, and Severs NJ.** Connexin45, a major connexin of the rabbit sinoatrial node, is co-expressed with connexin43 in a restricted zone at the nodal-crista terminalis border. *J Histochem Cytochem* 47: 907–918, 1999.
12. **Davis LM, Rodefeld ME, Green K, Beyer EC, and Saffitz JE.** Gap junction protein phenotypes of the human heart and conduction system. *J Cardiovasc Electrophysiol* 6: 813–822, 1995.
13. **Delorme B, Jary-Guichard T, Briand JP, Willecke K, Gros D, and Theveniau-Ruissy M.** Expression pattern of connexin gene products at the early developmental stages of the mouse cardiovascular system. *Circ Res* 81: 423–437, 1997.
14. **Denyer JC and Brown HF.** Rabbit sinoatrial node cells: isolation and electrophysiological properties. *J Physiol (Lond)* 428: 405–424, 1990.
15. **Difrancesco D, Ferroni A, Mazzanti M, and Tromba C.** Properties of the hyperpolarizing-activated current (I_f) in cells isolated from the rabbit sinoatrial node. *J Physiol (Lond)* 377: 61–88, 1986.
16. **Ebihara L, Xu X, Oberti C, Beyer EC, and Berthoud VM.** Co-expression of lens fiber connexins modifies hemi-gap-junctional channel behavior. *Biophys J* 76: 198–206, 1999.
17. **El Aoumari A, Fromaget C, Dupont E, Reggio H, Durbec P, Briand JP, Beller K, Kreitman B, and Gros D.** Conservation of a cytoplasmatic carboxy terminal domain of Cx43, a gap junction protein, in mammal heart and brain. *J Membr Biol* 115: 229–240, 1990.
18. **Goodenough DA, Goliger JA, and Paul DL.** Connexins, connexons and intercellular communication. *Annu Rev Biochem* 65: 475–502, 1996.
19. **Gorza L and Vitadello M.** Distribution of conduction system fibers in the developing and adult rabbit heart revealed by an antineurofilament antibody. *Circ Res* 65: 360–369, 1989.
20. **Gros D and Jongsma HJ.** Connexins in mammalian heart function. *Bioessays* 18: 719–730, 1996.
21. **Guo J, Ono K, and Noma A.** A sustained inward current activated at the diastolic potential range in rabbit sinoatrial node cells. *J Physiol (Lond)* 483: 1–13, 1995.
22. **Habuchi Y, Lu L-L, Morikawa J, and Yoshimura M.** Angiotensin II inhibition of L-type Ca^{2+} current in sinoatrial node cells of rabbits. *Am J Physiol Heart Circ Physiol* 268: H1053–H1060, 1995.
23. **Haefliger J-A, Bruzzone R, Jenkins NA, Gilbert DJ, Copeland NG, and Paul DL.** Four novel members of the connexin family of gap junction proteins. *J Biol Chem* 267: 2057–2064, 1992.
24. **He DS, Jiang JX, Taffet SM, and Burt JM.** Formation of heteromeric gap junction channels by connexins 40 and 43 in vascular smooth muscle cells. *Proc Natl Acad Sci USA* 96: 6495–6500, 1999.
25. **Jalife J.** Mutual entrainment and electrical coupling as mechanisms of synchronous firing of rabbit sinoatrial pace-maker cells. *J Physiol (Lond)* 356: 221–243, 1989.
26. **Joyner RW and van Capelle FJL.** Propagation through electrically coupled cells: how a small SA node drives a large atrium. *Biophys J* 50: 1157–1164, 1986.
27. **Kanter HL, Saffitz JE, and Beyer EC.** Cardiac myocytes express multiple gap junction proteins. *Circ Res* 70: 438–444, 1992.
28. **Kempen MJA van, Fromaget C, Gros D, Moorman AFM, and Lamers WH.** Spatial distribution of connexin43, the major cardiac gap junction protein, in the developing and adult rat heart. *Circ Res* 68: 1638–1651, 1991.
29. **Kempen MJA van, ten Velde I, Wessels A, Oosthoek PW, Gros D, Jongsma HJ, Moorman AFM, and Lamers WH.** Differential connexin distribution accommodates cardiac function in different species. *Microsc Res Tech* 420–436: 1995.
30. **Kirchhof CJHJ, Bonke FIM, Allessie MA, Roos AGJM, and Lammers WJEP.** An easy and direct approach to investigate conduction properties of the rabbit sinus node. *J Cardiovasc Pharmacol* 11: 667–675, 1988.
31. **Kwong KF, Schuessler RB, Green KG, Laing JG, Beyer EC, Boineau JP, and Saffitz JE.** Differential expression of gap junction proteins in the canine sinus node. *Circ Res* 82: 604–612, 1998.
32. **Masson Pévet M, Bleeker WK, and Gros D.** The plasma membrane of leading pacemaker cells in the rabbit sinus node: a

qualitative and quantitative ultrastructural analysis. *Circ Res* 45: 621–629, 1979.

33. **Michaels DC, Matyas EP, and Jalife J.** Mechanisms of pacemaker synchronization: a new hypothesis. *Circ Res* 61: 704–714, 1987.
34. **Moreno AP, Laing JG, Beyer EC, and Spray DC.** Properties of gap junction channels formed of connexin45 endogenously expressed in human hepatoma (SKHep1) cells. *Am J Physiol Cell Physiol* 268: C356–C365, 1995.
35. **Moreno AP, Rook MB, Fishman GI, and Spray DC.** Gap junction channels: distinct voltage-sensitive and -insensitive states. *Biophys J* 67: 113–119, 1994.
36. **Neyton J and Trautmann A.** Single channel currents of an intercellular junction. *Nature* 317: 331–335, 1985.
37. **Oosthoek PW, Viragh S, Mayen AEM, van Kempen MJA, Lamers WH, and Moorman AFM.** Immunohistochemical delineation of the conduction system. I. The sinoatrial node. *Circ Res* 73: 473–481, 1993.
38. **Opthof T.** Gap junctions in the sinoatrial node: immunohistochemical localization and correlation with activation pattern. *J Cardiovasc Electrophysiol* 5: 138–143, 1994.
39. **Opthof T, de Jonge B, Mackaay AJC, Bleeker WK, Masson-Pévet M, Jongsma HJ, and Bouman LN.** Functional and morphological organization of the guinea pig sinoatrial node compared with the rabbit sinoatrial node. *J Mol Cell Cardiol* 17: 549–564, 1985.
40. **Paul DL, Ebihara L, Takemoto LJ, Swenson KI, and Goodenough DA.** Connexin46, a novel lens gap junction protein, induces voltage-gated currents in nonjunctional plasma membrane of *Xenopus* oocytes. *J Cell Biol* 115: 1077–1089, 1991.
41. **Reed KE, Westphale EM, Larson DM, Wang H-Z, Veenstra RD, and Beyer EC.** Molecular cloning and functional expression of human connexin37, an endothelial gap junction protein. *J Clin Invest* 91: 997–1004, 1993.
42. **Rijen HVM van, Wilders R, van Ginneken ACG, and Jongsma HJ.** Quantitative analysis of dual whole-cell voltage-clamp determination of gap junctional conductance. *Pflügers Arch* 430: 141–151, 1998.
43. **Takens-Kwak BR, Sáez Wilders JCR, Chanson M, Fishman GI, Herzberg EL, Spray DC, and Jongsma HJ.** Effects of cGMP-dependent phosphorylation on rat and human connexin43 gap junction channels. *Pflügers Arch* 430: 770–778, 1995.
44. **Trabna-Janik E, Coombs W, Lemanski LF, Delmar M, and Jalife J.** Immunohistochemical localization of gap junction protein channels in hamster sinoatrial node in correlation with electrophysiologic mapping of the pacemaker region. *J Cardiovasc Electrophysiol* 5: 125–137, 1994.
45. **Traub O, Eckert R, Lichtenberg-Fraté H, Elfgang C, Bastide B, Scheidtmann KH, Hülser DF, and Willecke K.** Immunochemical and electrophysiological characterization of murine connexin40 and -43 in mouse tissues and transfected human cells. *Eur J Cell Biol* 64: 101–112, 1994.
46. **Trexler EB, Bennett MVL, Bargiello TA, and Verselis VK.** Voltage gating and permeation in a gap junction hemichannel. *Proc Natl Acad Sci USA* 93: 5836–5841, 1996.
47. **Velde I ten, de Jonge B, Verheijck EE, van Kempen MJA, Analbers L, Gros D, and Jongsma HJ.** Spatial distribution of connexin43, the major cardiac gap junction protein, visualizes the cellular network for impulse propagation from sinoatrial node to atrium. *Circ Res* 76: 802–811, 1995.
48. **Verheijck EE, Wessels A, van Ginneken ACG, Bourier J, Markman MWM, Vermeulen JLM, de Bakker JMT, Lamers WH, Opthof T, and Bouman LN.** Distribution of atrial and nodal cells within the rabbit sinoatrial node. *Circulation* 97: 1623–1631, 1998.
49. **Verheijck EE, Wilders R, Joyner RW, Golod DA, Kumar R, Jongsma HJ, Bouman LN, and van Ginneken ACG.** Pacemaker synchronization of electrically coupled rabbit sinoatrial node cells. *J Gen Physiol* 11: 95–112, 1998.
50. **Verheule S, van Kempen MJA, te Welscher PHJA, Kwak BR, and Jongsma HJ.** Characterization of gap junction channels in adult rabbit atrial and ventricular myocardium. *Circ Res* 80: 673–681, 1997.
51. **White RL, Spray DC, Campos de Carvalho AC, Wittenberg BA, and Bennet MLV.** Some electrical and pharmacological properties of gap junctions between adult ventricular myocytes. *Am J Physiol Cell Physiol* 249: C447–C455, 1985.
52. **White TW, Bruzzone R, Wolfram S, Paul DL, and Goodenough DA.** Selective interactions among multiple connexin proteins expressed in the vertebrate lens: the second extracellular domain is a determinant of compatibility between connexins. *J Cell Biol* 125: 879–892, 1994.
53. **White TW, Paul DL, Goodenough DA, and Bruzzone R.** Functional analysis of selective interactions among rodent connexins. *Mol Biol Cell* 6: 459–470, 1995.
54. **Wilders R and Jongsma HJ.** Limitations of the dual voltage clamp method in assaying conductance and kinetics of gap junction channels. *Biophys J* 63: 942–953, 1992.
55. **Wilders R, Jongsma HJ, and van Ginneken ACG.** Pacemaker activity of the rabbit sinoatrial node: a comparison of mathematical models. *Biophys J* 60: 1202–1216, 1991.
56. **Wilders R, Verheijck EE, Kumar R, Goolsby WN, van Ginneken ACG, Joyner RW, and Jongsma HJ.** Model clamp and its application to synchronization of rabbit sinoatrial node cells. *Am J Physiol Heart Circ Physiol* 271: H2168–H2182, 1996.